JACS
JOURNAL OF THE AMERICAN CHEMICAL SOCIETY

Article

pubs.acs.org/JACS

Mechanism of Charge Transfer and Recombination Dynamics in Organo Metal Halide Perovskites and Organic Electrodes, PCBM, and Spiro-OMeTAD: Role of Dark Carriers

Carlito S. Ponseca Jr.,[*,†] Eline M. Hutter,[‡] Piotr Piatkowski,[§] Boiko Cohen,[§] Torbjörn Pascher,[†] Abderrazzak Douhal,[§] Arkady Yartsev,[†] Villy Sundström,[*,†] and Tom J. Savenije[‡]

[†]Division of Chemical Physics, Lund University, Box 124, 221 00 Lund, Sweden

[‡]Department of Chemical Engineering, Delft University of Technology, 2628 BL Delft, The Netherlands

[§]Departamento de Quimica Fisica, Facultad de Ciencias Ambientales y Bioquimica, and INAMOL, Universidad de Castilla-La Mancha, Avenida Carlos III, S/N, 45071 Toledo, Spain

Supporting Information

ABSTRACT: Despite the unprecedented interest in organic−inorganic metal halide perovskite solar cells, quantitative information on the charge transfer dynamics into selective electrodes is still lacking. In this paper, we report the time scales and mechanisms of electron and hole injection and recombination dynamics at organic PCBM and Spiro-OMeTAD electrode interfaces. On the one hand, hole transfer is complete on the subpicosecond time scale in $MAPbI_3$/Spiro-OMeTAD, and its recombination rate is similar to that in neat $MAPbI_3$. This was found to be due to a high concentration of dark charges, i.e., holes brought about by unintentional p-type doping of $MAPbI_3$. Hence, the total concentration of holes in the perovskite is hardly affected by optical excitation, which manifested as similar decay kinetics. On the other hand, the decay of the photoinduced conductivity in $MAPbI_3$/PCBM is on the time scale of hundreds of picoseconds to several nanoseconds, due to electron injection into PCBM and electron−hole recombination at the interface occurring at similar rates. These results highlight the importance of understanding the role of dark carriers in deconvoluting the complex photophysical processes in these materials. Moreover, optimizing the preparation processes wherein undesired doping is minimized could prompt the use of organic molecules as a more viable electrode substitute for perovskite solar cell devices.

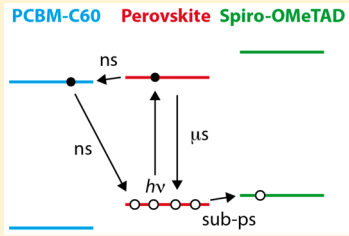

INTRODUCTION

The need for understanding the fundamental photophysical processes in organo metal halide perovskite (OMHP) solar cells has become more evident in view of the swift rise in efficiency of these devices.[1−6] However, literature provides limited details of the charge carrier dynamics, i.e., from charge generation to transport and finally their extraction to the electrodes. We and others have reported injection of electrons from OMHPs to TiO_2 just only very recently.[6−8] Other time-resolved studies have started to reveal several other unique properties of this material, e.g., high mobilities of electrons and holes,[9] slow recombination of charges,[2,6,10] and diffusion lengths of micrometers.[6,11] Although theoretical calculations indicate balanced electron and hole mobilities,[12−14] different groups report widely varying values for electron and hole mobilities in the perovskite.[7,15] Additionally, it is unclear to what extent OMHPs can be regarded as genuine intrinsic semiconductors. Recent research has pointed out that under specific preparation conditions OMHPs may behave as n-type[16−18] or p-type semiconductor.[18−21] It is therefore necessary to determine the role of dark carriers in understanding its photophysical properties.

In this study, we report on the electron and hole injection and recombination dynamics of two frequently used charge-specific organic electrodes: the electron acceptor [6,6]-phenyl-C61-butyric acid methyl ester, PCBM, and the hole acceptor Spiro-OMeTAD.[8,11,22−24] Thin polycrystalline films of $MAPbI_3$ were prepared by spin-coating CH_3NH_3I and PbI_2 in a stoichiometric ratio from a γ-butyrolactone solution in a nitrogen-filled glovebox. Results of XRD measurements showing tetragonal structure of the perovskite can be found in Figure S1. PCBM or Spiro-OMeTAD was spin-coated the on top of the $MAPbI_3$. All samples have not been exposed to ambient conditions at any time before and during the electrical measurements. By time-resolved, electrodeless conductivity measurements, using terahertz (THz) or microwave (MW) radiation as probe, we are able to monitor the photoinduced charge carrier formation and decay from subpicosecond time scales up to one microsecond. We note that the instrument response function (IRF) of our THz setup is about 0.2 ps, whereas for MW it is 18 ns. Moreover, because of the superior signal-to-noise of the MW setup, the excitation densities that can be used are at least an order of magnitude lower than those for time-resolved THz spectroscopy (TRTS). Other details of the growth method, cross-sectional SEM images of the samples,

Received: July 3, 2015
Published: December 4, 2015

DOI: 10.1021/jacs.5b08770
J. Am. Chem. Soc. 2015, 137, 16043−16048

and the description of the time-resolved techniques can be found in the Supporting Information.

We found that on optical excitation of the perovskite, charge transfer from $MAPbI_3$ into Spiro-OMeTAD occurs on the subpicosecond time scale but is much slower, from few hundreds of picoseconds to several nanoseconds, with PCBM as electron-accepting electrode. The difference in the injection rate was assigned to differences in energy band alignment at the interface. Furthermore, by using the photoinduced time-resolved microwave conductivity (TRMC) technique, the charge carrier recombination back to the ground state was found to be at least 1 order of magnitude faster in the $MAPbI_3$/PCBM (few nanoseconds to few tens of nanoseconds) than in the $MAPbI_3$/Spiro-OMeTAD (hundreds of nanoseconds to several microseconds). We surmise that this faster decay in $MAPbI_3$/PCBM is due to interfacial recombination between electrons injected into PCBM with both photoinduced and dark holes in $MAPbI_3$. For the $MAPbI_3$/Spiro-OMeTAD, the photoexcited electrons undergo a decay route similar to that in the neat $MAPbI_3$. This suggests that the total concentration of holes in $MAPbI_3$ does not appreciably change upon injection of photogenerated holes into Spiro-OMeTAD. Altogether, our results suggest that the $MAPbI_3$ studied here is an unintentionally p-type doped semiconductor, which controls the charge carrier dynamics into organic electrodes.

RESULTS AND DISCUSSION

Plotted in Figure 1a are the TRTS kinetics of neat $MAPbI_3$, $MAPbI_3$/PCBM, and $MAPbI_3$/Spiro-OMeTAD. The samples are excited at 590 nm through the organic layer, which at this wavelength does not substantially absorb the incident laser light. Although the $MAPbI_3$ layer consists of large, micrometer-sized granular structures according to surface profilometry, the light penetration depth at this wavelength into $MAPbI_3$ is only about 200 nm.[26] The TRTS signal is expressed as the product of the quantum yield, φ, and the sum of electron and hole mobility ($\mu_e + \mu_h$). This product is calculated according to

$$\varphi(\mu_e + \mu_h) = \frac{\Delta\sigma L}{eI_0F_A} \quad (1)$$

where $\Delta\sigma$ is the measured change in conductivity, L is the thickness, e is the elementary charge, I_0 is the number of photons per unit area per pulse, and F_A is the fraction of absorbed light. The value of φ is assumed to be close to unity at short time scales. Analogous to our previous work,[6,25] the maximum initial signal size for the neat $MAPbI_3$ is ~15 $cm^2/(V\,s)$ because of ($\mu_e + \mu_h$). After 1 ns, the signal has slightly decayed because of second-order recombination as reported previously.[6] Interestingly, the samples with acceptor layers show a very different behavior. For $MAPbI_3$/PCBM, the initial signal size is similar to that of the neat $MAPbI_3$ but decays much faster. This rapid decay is clearly seen on a 7 ns time window (Figure 1b). For $MAPbI_3$/Spiro-OMeTAD, the TRTS signal is about three times smaller than that for neat $MAPbI_3$, close to 5 $cm^2/(V\,s)$ and approximately constant over the first nanoseconds.

Figure 2a shows the TRMC kinetics of the three samples. The maximum signal heights are normalized to 1 to allow comparison of the decay kinetics. Most prominent is that the $MAPbI_3$/PCBM shows rapid decay kinetics, whereas the two other samples show a nearly identical, much slower decay comparable to previously reported decays.[7] In Figure 2b, the

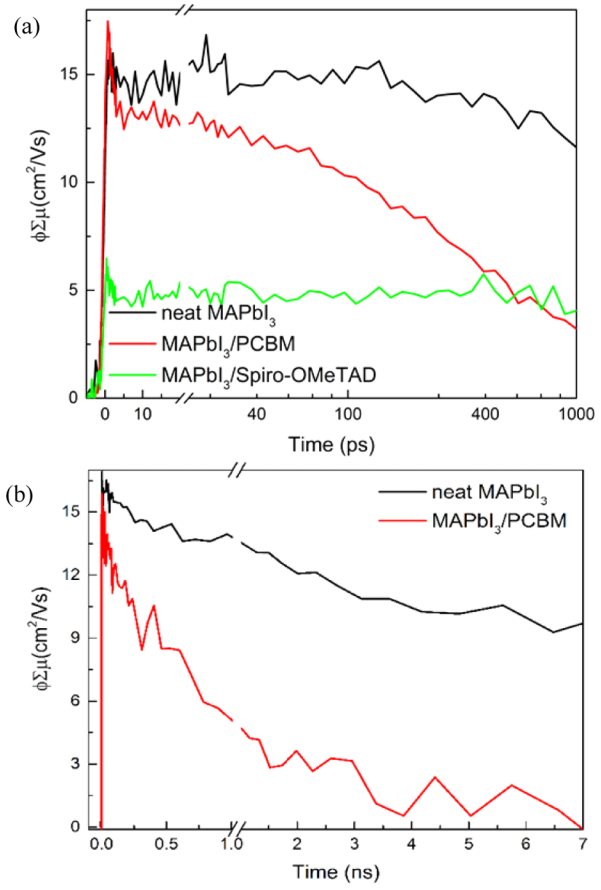

Figure 1. TRTS photoconductivity kinetics of (a) neat $MAPbI_3$, $MAPbI_3$/PCBM, and $MAPbI_3$/Spiro-OMeTAD for 1 ns and (b) $MAPbI_3$ and $MAPbI_3$/PCBM for 7 ns, normalized to the excitation intensity of 2.1×10^{12} and 8.0×10^{12} ph/cm^2 per pulse, respectively (λ_{pump} = 590 nm).

maximum signal amplitudes, expressed as $\varphi(\mu_e + \mu_h)$, are plotted versus the incident photon flux. For the neat $MAPbI_3$ layer, $\varphi(\mu_e + \mu_h)$ decreases on increasing fluences (for $I_0 > 4 \times 10^{11}$ ph/cm^2) that was assigned to second-order electron–hole recombination similar to previous reports.[6,10,25] However, there may be other processes that could also influence the decay in TRMC kinetics. Using the model in our previous work,[27] both background doping (10^{15} cm^{-3}) and photodoping were considered; the latter is a result of electron trapping and, as a consequence, is highly dependent on the concentration of electron traps. From the results of the model, it can be deduced that trapping is important up to excitation intensity of about 10^{11} ph/cm^2, whereas second-order recombination is the dominant decay pathway at higher excitation intensities as shown in Figure S2. Hence, below this intensity threshold, $\varphi(\mu_e + \mu_h)$ values remain constant. This also explains the overlapping of traces observed at low light fluences (Figure S1). Figure 2b also shows that the TRMC signals are substantially smaller for the samples with acceptor layers than those of the neat $MAPbI_3$ and that they decrease with increasing fluences. For $MAPbI_3$/PCBM the threshold for this process is shifted to higher fluence (>10^{12} ph/cm^2).

Spiro-OMeTAD has been extensively used as a hole-transporting material (HTM) and has an offset in the valence band of approximately 0.57 eV with respect to $MAPbI_3$.[8,22,29,30] However, additives like lithium bis(trifluoromethanesulfonyl)

DOI: 10.1021/jacs.5b08770
J. Am. Chem. Soc. 2015, 137, 16043–16048

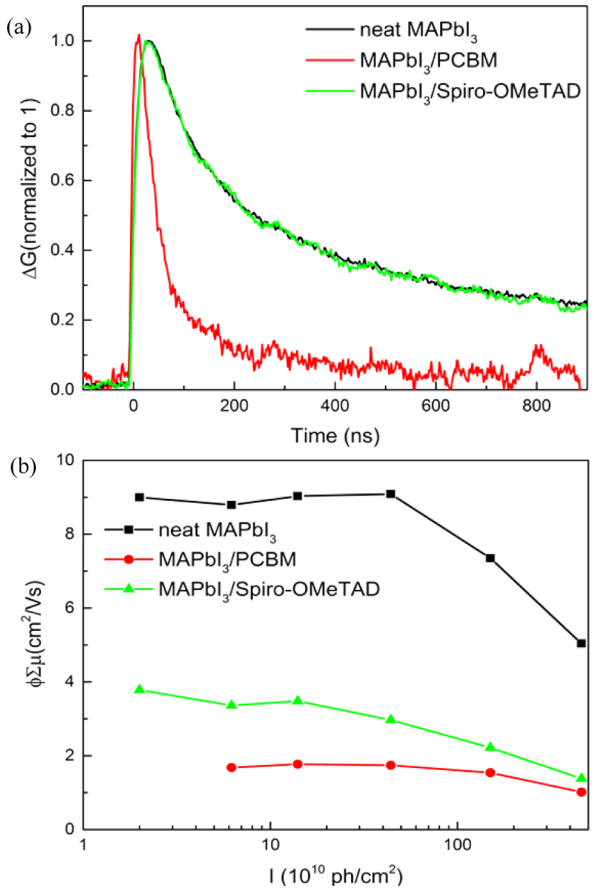

Figure 2. (a) TRMC traces for the three samples recorded at an excitation intensity of 1.0×10^{11} photons/cm^2 per pulse (λ_{pump} = 600 nm), normalized to unity. (b) Product of φ times ($\mu_e + \mu_h$) versus incident intensity of the three samples.

imide (LiTFSI) are required to substantially increase the very low intrinsic conductivity in this HTM, i.e., 10^{-8} S/cm.[32] The use of additives then leads to decent overall power conversion efficiency (PCE).[22,31,33] The mobility measured in the $MAPbI_3$/Spiro-OMeTAD sample using TRTS is 5 cm^2/(V s), which is three times lower than that in neat $MAPbI_3$ (15 cm^2/(V s)). Similarly, the mobility obtained from TRMC decreased from 9 cm^2/(V s) in neat $MAPbI_3$ to 3.5 cm^2/(V s) in $MAPbI_3$/Spiro-OMeTAD (Figure 2b). The reduction of the signal can be interpreted as disappearance of one of the two photogenerated species from the neat $MAPbI_3$ as a result of charge injection. Because Spiro-OMeTAD is an HTM, it should be the holes that disappeared and therefore were injected. The hole transfer is confirmed by both techniques, and the time scale of injection is subpicoseconds as seen by TRTS. Recent transient absorption spectroscopy results also agree with this time scale of hole injection (0.7 ps).[36] This ultrafast injection shows that the energy offset at the interface alone is enough to allow efficient subpicosecond hole injection despite the fact that in our experiments no additive was used. Moreover, this means that the mobilities measured by the two techniques in the $MAPbI_3$/Spiro-OMeTAD, 5 cm^2/(V s) in TRTS and 3.5 cm^2/(V s) in TRMC originate from the electrons left in the $MAPbI_3$ as shown in Scheme 1. This leads to a THz hole mobility of 10 cm^2/(V s) (and MW hole mobility of 5.5 cm^2/(V s)) in the neat $MAPbI_3$ perovskite. Diffusion-controlled motion of the light-induced carriers generated within the perovskite layer also

Scheme 1. Schematic of Energy Levels of Perovskite, Spiro-OMeTAD, and PCBM Showing Photo-Physical Processes[a]

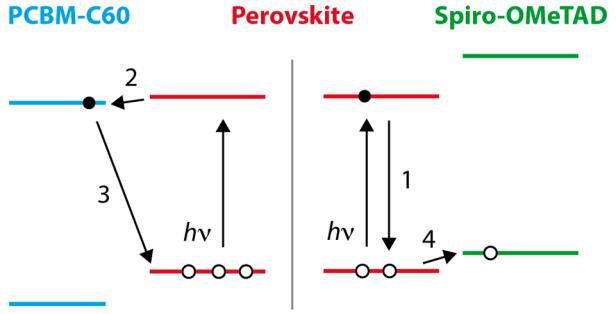

[a]1: (Non-geminate) electron hole recombination, 2: electron injection, 3: interfacial electron hole recombination, 4: hole injection, and 5: interfacial electron hole recombination.

points to a subnanosecond time scale for hole collection at the $MAPbI_3$/Spiro-OMeTAD interface. Furthermore, selectively exciting the perovskite through the organic accepting layer results in most of the carriers being generated close to the granular perovskite interface. These facts together with large driving force lead to an expected picosecond time scale for the hole injection from the perovskite into the Spiro-OMeTAD layer. We note that the ratio of electron and hole mobilities obtained here do not differ by more than a factor of two, in line with previous conclusions on the balanced transport of charges in these materials.[4,6]

The above picture, however, is not sufficient to rationalize the similarity in the TRMC decay kinetics of neat $MAPbI_3$ and $MAPbI_3$/Spiro-OMeTAD. It should be stressed that not only at low fluence the decays of kinetics are identical, but also at other higher incident intensities (Figure S2). In the past, we have seen that charge transfer over an interface typically leads to different decay kinetics as compared to the dynamics of carriers generated in a single semiconductor.[34] The identical TRMC kinetics shown in Figure 2a, suggest that the decay pathways for the photoinduced mobile charges in the neat $MAPbI_3$ and in the $MAPbI_3$/Spiro-OMeTAD must be very similar if not identical. To explain this behavior, we postulate that the perovskite has a concentration of holes already in the dark (p_0), i.e., that $MAPbI_3$ is an unintentionally doped, p-type semiconductor. On optical excitation, excess charge carriers are formed instantaneously, and holes are transferred to Spiro-OMeTAD. Electrons left in the conduction band of $MAPbI_3$ then recombine with both the dark holes in the valence band of $MAPbI_3$ and the photogenerated holes injected into Spiro-OMeTAD. However, as long as the concentration of photogenerated electrons is smaller than the total concentration of holes (dark and light-induced carriers), the electron hole recombination kinetics in $MAPbI_3$ are barely dependent on whether holes are transferred to the Spiro-OMeTAD or not. Hence, the resulting conductivity decay of the $MAPbI_3$/Spiro-OMeTAD follows the same kinetics as that in neat $MAPbI_3$, i.e., a few hundreds of nanoseconds. The fact that we see a slight change in the decay kinetics at only the highest excitation densities of 1.5×10^{12} ph/cm^2 yielding an initial charge carrier concentration of about 7.5×10^{16} cm^{-3} within the $MAPbI_3$ suggests that p_0 should be at least 10^{16} cm^{-3}. This is in agreement with previous estimates for p_0 in $MAPbI_3$.[27] One should note that both TRTS and TRMC probe only the change

DOI: 10.1021/jacs.5b08770
J. Am. Chem. Soc. 2015, 137, 16043−16048

in conductivity due to optical excitation but not the dark conductivity.

PCBM used as an electron-specific electrode in $MAPbI_3$ solar cells, despite its small driving energies for electron injection, has been reported to have PCEs of over 10%.[23,37] This indicates that electrons are transferred from the perovskite to PCBM (process 2, Scheme 1) as part of the charge extraction process. The TRTS and TRMC kinetics contain information about this, but as illustrated in Scheme 1, there are several processes that could contribute to a decay of conductivity. The electron mobility in PCBM is quite small, i.e., 10^{-3} $cm^2/(V\ s)$,[37−41] and therefore contributes insignificantly to the photoconductivity signal of both techniques. In other words, the measured signals only represent the mobile photogenerated electrons and holes in the perovskite. This implies that electron injection from $MAPbI_3$ to PCBM (process 2, Scheme 1), recombination at the $MAPbI_3$/PCBM interface (process 3, Scheme 1), and recombination within the $MAPbI_3$ (process 1, Scheme 1) will lead to a decay in the measured photoconductivity. As a starting point to disentangle the contributions of processes 1−3 to the observed kinetics, the following qualitative consideration can be made. One possible scenario is that the electron injection (process 2, Scheme 1) is much faster than interfacial recombination between electrons in PCBM and holes in the perovskite (process 3, Scheme 1). In this case, a clear nonexponential, slower decay with reduced signal amplitude is expected because mobile electrons in $MAPbI_3$ become immobile in PCBM. Because we do not observe such a plateau, more clearly shown in Figure 1b, we can conclude that the rate constant for the interfacial electron hole recombination (process 3, Scheme 1) is similar to or exceeds the electron injection rate. This is consistent with the fact that the driving force for electron injection is small.

We now examine in more detail the measured TRTS and TRMC kinetics. At the earliest time scale, the THz conductivity signal of the $MAPbI_3$/PCBM and neat $MAPbI_3$ is the same (∼15 $cm^2/(V\ s)$, Figure 1a), showing that mobile charges are formed rapidly (<1 ps) and that the photogenerated charges stay in the perovskite for at least a few picoseconds. At a 1 ns delay, the TRTS signal is reduced by approximately a third, suggesting that charges are disappearing on this time scale. Within the framework of Scheme 1, three different processes, either consecutively or simultaneously occurring, may be responsible for this decay. First, unlike in $MAPbI_3$/Spiro-OMeTAD where there is a 0.57 eV driving force favoring subpicosecond hole injection, here there is a smaller energy offset at the interface between $MAPbI_3$ and PCBM (0.3 eV).[4,42] This could retard electron injection from few hundreds of picoseconds to nanoseconds time domain. Electron injection from perovskite to PCBM as reported by Xing et al. using transient absorption spectroscopy falls within this time scale (0.4 ps).[4] The THz decay can therefore be assigned to disappearance of electrons in $MAPbI_3$, i.e., injection into PCBM. Second, because the perovskite used in $MAPbI_3$/PCBM was prepared under the same conditions as those of $MAPbI_3$/Spiro-OMeTAD, we expect a similar concentration of dark holes in both samples. After injection into PCBM, electrons stay close to the $MAPbI_3$/PCBM interface because of the low mobility in PCBM. This will inevitably lead to recombination with dark and photogenerated holes in the $MAPbI_3$ and, as mentioned above, could manifest as decay in the TRTS kinetics as well. The third process that could potentially be causing decay of the conductivity signal is second-order recombination within the perovskite. The THz kinetics of neat $MAPbI_3$, Figure 1a,b, shows that at the excitation intensity used this process occurs significantly more slowly than does the decay of the $MAPbI_3$/PCBM conductivity. Thus, second-order recombination only weakly contributes. The TRTS conductivity decay is therefore a convolution of electron injection to PCBM and electron hole recombination at the perovskite/PCBM interface, with both processes occurring on a similar time scale.

The TRMC measurements extend the time window of the conductivity measurements to hundreds of nanoseconds and can be performed at lower excitation intensity than the TRTS, Figure 2a. In this case, second-order recombination occurs on the microsecond time scale[25] and will contribute marginally to the observed decay. Hence, the observed TRMC decay is only a result of electron injection and interfacial recombination. The decay on the several tens of nanoseconds scale seen in Figures 2a and S4 is however significantly influenced by the 18 ns IRF of the TRMC measurement. This is apparent from the comparison of MW conductivity decay measured with an open- and closed-cell configuration (Figure S5), the former having a shorter IRF, i.e., ∼3 ns. The TRMC signal in the open-cell measurement decays to ∼50% of the peak amplitude within ∼20 ns, showing that the TRTS and TRMC measurements are converging toward a decay of photoconductivity on the hundreds of picoseconds and nanoseconds time scale. Any remaining discrepancy between the two techniques can be traced to the IRF of the open-cell TRMC measurement, which cannot catch the fastest 100 ps time scale of the decay, and lower excitation intensity in the TRMC measurements, decreasing the contribution to the decay of second-order recombination within the perovskite. Details explaining the difference between the open- and closed-cell measurements can be found in the Supporting Information.

Wojciechowski et al. reported TRMC kinetics similar to that observed here but assigned the decay only to electron injection from perovskite to PCBM. However, their model required that the hole mobility is an order of magnitude lower than the electron mobility.[7] This is in contrast with (1) several theoretical papers on the effective masses of electrons and holes stating that they do not differ more than a factor of two,[12−14] (2) experimental works showing balanced electron−hole diffusion lengths,[4,11] and (3) previous THz and TRMC conductivity measurements.[6,25] Our results, however, show that it is possible to explain the TRMC kinetics as slow (hundreds of picoseconds to nanoseconds) electron injection into PCBM, in convolution with interfacial recombination between immobile electrons in PCBM and photogenerated and dark holes in the perovskite. The resulting picture of this interpretation is an oppositely charged bilayer sample whose recombination dynamics is not influenced by the excitation density. Indeed, as shown in Figure S5, the decay kinetics of $MAPbI_3$/PCBM has a strong pseudo-first-order character due to the high concentration of p_0 (10^{16} cm^{-3}). Finally, our interpretation of the time-resolved decay kinetics in $MAPbI_3$/PCBM is consistent with the balanced electron and hole mobilities in $MAPbI_3$ reported in the literature.[4] It should be stressed though that the concentration of dark charges (either electrons or holes) is contingent upon the conditions under which the samples are prepared, e.g., thermal annealing. Wang et al. showed that annealing (time and temperature) can convert a perovskite from p- to n-type, and the carrier (dopant)

DOI: 10.1021/jacs.5b08770
J. Am. Chem. Soc. 2015, 137, 16043−16048

concentration can be varied as much as 6 orders of magnitude.[43]

By using transient photoluminescence (PL), Xing et al.[4] and Stranks et al.[11] reported the time scale of PL decay in neat $MAPbI_3$ as well as electron and hole injection to PCBM and Spiro-OMeTAD, respectively. The decay rate in neat $MAPbI_3$ is about 50 ns, and the injection rates for electrons and holes are substantially faster. PL from perovskites originates from the radiative band-to-band recombination of opposite carriers as extensively described by Stranks et al.[45] As shown in that paper, there are many higher order, nonradiative processes occurring, including trapping and recombination with photodoped background carriers, demonstrating the difficulty of revealing the complex photophysics of these materials from PL decay alone. In this work and in our previous reports,[6,25] we show that charges remain highly mobile up to at least 5 μs, which is at least 2 orders longer than the lifetimes measured by PL (refs 4 and 5). This is a strong indication that there is a population of charge carriers that does not recombine radiatively and that TRTS and TRMC are the appropriate tools to probe carrier dynamics from the picosecond to microsecond time scale. Admittedly, the exact time scale of carrier dynamics are highly excitation and sample dependent, and for direct comparison, one should measure under exactly identical conditions and from the same sample.

These results have far reaching implications both in understanding the fundamental photophysical processes of these materials as well as the operation of perovskite solar cells. Utmost care should be taken in interpreting photophysical data because it is strongly influenced by the nature and population of defects that controls its doping. This is exemplified by our recent work wherein we showed that different preparation procedures can lead to very different hole concentrations.[27] For solar cell operation, the relatively fast recombination at the $MAPbI_3$/PCBM interface represents a loss mechanism and could lead to a lower photocurrent. In efficient perovskite devices, rapid collection of holes by Spiro-OMeTAD helps avoid this loss mechanism. Furthermore, fast removal of electrons from the $MAPbI_3$/PCBM interface by, for example, increasing the conductivity in PCBM could help in reducing interfacial recombination. Most probably, the best method to avoid interfacial recombination is reduction of the unintentional high concentration of dark holes in the perovskite. The p-type doping might find its origin in defects in the $MAPbI_3$ crystal lattice such as vacancies.[17,20,44] Additionally, extrinsic dopants might be present because of impurities in the PbI_2 precursor. For the development of high-efficiency solar cells, it is imperative to reveal the relationship between preparation route and the electronic properties.

CONCLUSIONS

We found that upon optical excitation of $MAPbI_3$ hole transfer from $MAPbI_3$ into Spiro-OMeTAD occurs on a subpicosecond time scale as observed using TRTS. Recombination dynamics in this material with an organic acceptor is identical to that of neat $MAPbI_3$ and was shown to be controlled by a high concentration of dark holes. Injection of electrons from perovskite to PCBM occurs on the hundreds of picoseconds to few nanoseconds time scale, convoluted with the fast interfacial recombination between the electrons in PCBM and the photogenerated and dark holes in $MAPbI_3$. Reduction of the hole concentration in the perovskite could help to retard recombination, yielding a higher overall power conversion efficiency.

ASSOCIATED CONTENT

Supporting Information

The Supporting Information is available free of charge on the ACS Publications website at DOI: 10.1021/jacs.5b08770.

Details of experimental set up and SEM micrographs. (PDF)

AUTHOR INFORMATION

Corresponding Authors

*carlito.ponseca@chemphys.lu.se
*villy.sundstrom@chemphys.lu.se

Author Contributions

C.S.P. and E.M.H. contributed equally to the present work.

Notes

The authors declare no competing financial interest.

ACKNOWLEDGMENTS

This work was supported by the Swedish Energy Agency (STEM), the Swedish Research Council, the Knut&Alice Wallenberg foundation, the European Research Council (Advanced Investigator Grant to VS, 226136-VISCHEM), the nanometer Consortium at Lund University (nmc@LU), the Lund Laser Center, the UCLM, and the MINECO (MAT2011-25472).

REFERENCES

(1) Lee, M. M.; Teuscher, J.; Miyasaka, T.; Murakami, T. N.; Snaith, H. J. *Science* **2012**, *338*, 643−647.
(2) Heo, J. H.; Im, S. H.; Noh, J. H.; Mandal, T. N.; Lim, C.-S.; Chang, J. A.; Lee, Y. H.; Kim, H.; Sarkar, A.; Nazeeruddin, M. K.; Grätzel, M.; Seok, S., Il *Nat. Photonics* **2013**, *7*, 486−491.
(3) Burschka, J.; Pellet, N.; Moon, S.-J.; Humphry-Baker, R.; Gao, P.; Nazeeruddin, M. K.; Grätzel, M. *Nature* **2013**, *499*, 316−319.
(4) Xing, G.; Mathews, N.; Sun, S.; Lim, S. S.; Lam, Y. M.; Grätzel, M.; Mhaisalkar, S.; Sum, T. C. *Science* **2013**, *342*, 344−347.
(5) Etgar, L.; Gao, P.; Xue, Z.; Peng, Q.; Chandiran, A. K.; Liu, B.; Nazeeruddin, Md. K.; Grätzel, M. *J. Am. Chem. Soc.* **2012**, *134*, 17396−17399.
(6) Ponseca, C. S.; Savenije, T. J.; Abdellah, M.; Zheng, K.; Yartsev, A.; Pascher, T.; Harlang, T.; Chabera, P.; Pullerits, T.; Stepanov, A.; Wolf, J.-P.; Sundström, V. *J. Am. Chem. Soc.* **2014**, *136*, 5189−5192.
(7) Wojciechowski, K.; Stranks, S. D.; Abate, A.; Sadoughi, G.; Sadhanala, A.; Kopidakis, N.; Rumbles, G.; Li, C.-Z.; Friend, R. H.; Jen, A. K.-Y.; Snaith, H. J. *ACS Nano* **2014**, *8*, 12701−12709.
(8) Abrusci, A.; Stranks, S. D.; Docampo, P.; Yip, H.-L.; Jen, A. K.-Y.; Snaith, H. J. *Nano Lett.* **2013**, *13*, 3124−3128.
(9) Wehrenfennig, C.; Eperon, G. E.; Johnston, M. B.; Snaith, H. J.; Herz, L. M. *Adv. Mater.* **2014**, *26*, 1584−1589.
(10) Wehrenfennig, C.; Liu, M.; Snaith, H. J.; Johnston, M. B.; Herz, L. M. *Energy Environ. Sci.* **2014**, *7*, 2269−2275.
(11) Stranks, S. D.; Eperon, G. E.; Grancini, G.; Menelaou, C.; Alcocer, M. J. P.; Leijtens, T.; Herz, L. M.; Petrozza, A.; Snaith, H. J. *Science* **2013**, *342*, 341−344.
(12) Chang, Y.; Park, C.; Matsuishi, K. *J. Korean Phys. Soc.* **2004**, *44*, 889−893.
(13) Giorgi, G.; Fujisawa, J. I.; Segawa, H.; Yamashita, K. *J. Phys. Chem. Lett.* **2013**, *4*, 4213−4216.
(14) Quarti, C.; Mosconi, E.; De Angelis, F. *Chem. Mater.* **2014**, *26*, 6557−6569.
(15) Oga, H.; Saeki, A.; Ogomi, Y.; Hayase, S.; Seki, S. *J. Am. Chem. Soc.* **2014**, *136*, 13818−13825.

DOI: 10.1021/jacs.5b08770
J. Am. Chem. Soc. 2015, 137, 16043−16048

(16) Leijtens, T.; Stranks, S. D.; Eperon, G. E.; Lindblad, R.; Johansson, E. M. J.; Mcpherson, I. J.; Rensmo, H.; Ball, J. M.; Lee, M. M.; Snaith, H. J. *ACS Nano* **2014**, *8*, 7147−7155.
(17) Yin, W.-J.; Shi, T.; Yan, Y. *J. Phys. Chem. C* **2015**, *119*, 5253−5264.
(18) Stoumpos, C. C.; Malliakas, C. D.; Kanatzidis, M. G. *Inorg. Chem.* **2013**, *52*, 9019−9038.
(19) Takahashi, Y.; Hasegawa, H.; Takahashi, Y.; Inabe, T. *J. Solid State Chem.* **2013**, *205*, 39−43.
(20) Shi, T.; Yin, W.-J.; Yan, Y. *J. Phys. Chem. C* **2014**, *118*, 25350−25354.
(21) Kim, J.; Lee, S. H.; Lee, J. H.; Hong, K. H. *J. Phys. Chem. Lett.* **2014**, *5*, 1312−1317.
(22) Kim, H.-S.; Lee, C.-R.; Im, J.-H.; Lee, K.-B.; Moehl, T.; Marchioro, A.; Moon, S.-J.; Humphry-Baker, R.; Yum, J.-H.; Moser, J. E.; Grätzel, M.; Park, N.-G. *Sci. Rep.* **2012**, *2*, 591.
(23) Malinkiewicz, O.; Yella, A.; Lee, Y. H.; Espallargas, G. M.; Graetzel, M.; Nazeeruddin, M. K.; Bolink, H. J. *Nat. Photonics* **2013**, *8*, 128−132.
(24) Sun, S.; Salim, T.; Mathews, N.; Duchamp, M.; Boothroyd, C.; Xing, G.; Sum, T. C.; Lam, Y. M. *Energy Environ. Sci.* **2014**, *7*, 399−407.
(25) Savenije, T. J.; Ponseca, C. S.; Kunneman, L.; Abdellah, M.; Zheng, K.; Tian, Y.; Zhu, Q.; Canton, S. E.; Scheblykin, I. G.; Pullerits, T.; Yartsev, A.; Sundström, V. *J. Phys. Chem. Lett.* **2014**, *5*, 2189−2194.
(26) Green, M. A.; Ho-Baillie, A.; Snaith, H. J. *Nat. Photonics* **2014**, *8*, 506−514.
(27) Hutter, E. M.; Eperon, G. E.; Stranks, S. D.; Savenije, T. J. *J. Phys. Chem. Lett.* **2015**, *6*, 3082−3090.
(28) Yamada, Y.; Nakamura, T.; Endo, M.; Wakamiya, A.; Kanemitsu, Y. *J. Am. Chem. Soc.* **2014**, *136*, 11610−11613.
(29) Shen, Q.; Ogomi, Y.; Chang, J.; Tsukamoto, S.; Kukihara, K.; Oshima, T.; Osada, N.; Yoshino, K.; Katayama, K.; Toyoda, T.; Hayase, S. *Phys. Chem. Chem. Phys.* **2014**, *16*, 19984−19992.
(30) Edri, E.; Kirmayer, S.; Mukhopadhyay, S.; Gartsman, K.; Hodes, G.; Cahen, D. *Nat. Commun.* **2014**, *5*, 3461.
(31) Marchioro, A.; Teuscher, J.; Friedrich, D.; Kunst, M.; van de Krol, R.; Moehl, T.; Grätzel, M.; Moser, J.-E. *Nat. Photonics* **2014**, *8*, 250−255.
(32) Nguyen, W. H.; Bailie, C. D.; Unger, E. L.; McGehee, M. D. *J. Am. Chem. Soc.* **2014**, *136*, 10996−11001.
(33) Schulz, P.; Edri, E.; Kirmayer, S.; Hodes, G.; Cahen, D.; Kahn, A. *Energy Environ. Sci.* **2014**, *7*, 1377.
(34) Kroeze, J. E.; Savenije, T. J.; Vermeulen, M. J. W.; Warman, J. M. *J. Phys. Chem. B* **2003**, *107*, 7696−7705.
(35) Barnea-Nehoshtan, L.; Kirmayer, S.; Edri, E.; Hodes, G.; Cahen, D. *J. Phys. Chem. Lett.* **2014**, *5*, 2408−2413.
(36) Piatkowski, P.; Cohen, B.; Javier Ramos, F.; Di Nunzio, M.; Nazeeruddin, M. K.; Grätzel, M.; Ahmad, S.; Douhal, A. *Phys. Chem. Chem. Phys.* **2015**, *17*, 14674−14684.
(37) Gao, P.; Grätzel, M.; Nazeeruddin, M. K. *Energy Environ. Sci.* **2014**, *7*, 2448−2463.
(38) Von Hauff, E.; Dyakonov, V.; Parisi, J. *Sol. Energy Mater. Sol. Cells* **2005**, *87*, 149−156.
(39) Mihailetchi, V. D.; Xie, H.; De Boer, B.; Koster, L. J. A.; Blom, P. W. M. *Adv. Funct. Mater.* **2006**, *16*, 699−708.
(40) Warman, J. M.; De Haas, M. P.; Anthopoulos, T. D.; De Leeuw, D. M. *Adv. Mater.* **2006**, *18*, 2294−2298.
(41) Savenije, T. J.; Ferguson, A. J.; Kopidakis, N.; Rumbles, G. *J. Phys. Chem. C* **2013**, *117*, 24085−24103.
(42) Cui, J.; Yuan, H.; Li, J.; Xu, X.; Shen, Y.; Lin, H.; Wang, M. *Sci. Technol. Adv. Mater.* **2015**, *16*, 036004.
(43) Wang, Q.; Shao, Y.; Xie, H.; Lyu, L.; Liu, X.; Gao, Y.; Huang, J. *Appl. Phys. Lett.* **2014**, *105*, 163508.
(44) Yin, W.-J.; Shi, T.; Yan, Y. *Appl. Phys. Lett.* **2014**, *104*, 063903.
(45) Stranks, S. D.; Burlakov, V. M.; Leijtens, T.; Ball, J. H.; Goriely, A.; Snaith, H. J. *Phys. Rev. Appl.* **2014**, *2*, 034007.

DOI: 10.1021/jacs.5b08770
J. Am. Chem. Soc. 2015, 137, 16043−16048